High-pressure and high-temperature electrical resistivity of ferromagnetic transition metals: Nickel and iron

Mohammad Yousuf, P. Ch. Sahu, and K. Govinda Rajan

Materials Science Laboratory, Indira Gandhi Centre for Atomic Research, Kalpakkam 603 102, India

(Received 16 January 1986)

In this paper we report high-pressure and high-temperature electrical resistivity measurements on nickel and iron. It is observed that in nickel, the pressure coefficient of electrical resistivity changes sign and magnitude across the magnetic transition. The pressure coefficient of electrical resistivity for iron is normal and is almost independent of temperature. In nickel, the data analysis indicates that the temperature derivative of the electrical resistivity goes through a minimum at 20 kbar, which could be connected to the band-structure change and to a second-order transition. By invoking the idea of the exchange version of Baber scattering operative in paramagnetic nickel, we are able to account for the anomalous behavior of the pressure coefficient of electrical resistivity.

I. INTRODUCTION

In transition metals, electrons are distributed into partially filled s, p, and d bands.[1–5] Transport properties are attributed to the behavior of electrons in the sp bands, and the d electrons govern the static properties such as cohesive energy, melting point, bulk modulus, and specific heat.[6–8] Thus the d electrons in the transition metals are weakly localized as the width of the $3d$ band is of the same general magnitude as the relevant intra-atomic Coulomb interaction energy.[1–5,9] In the case of iron, nickel, and cobalt, it is observed that these itinerant d electrons also give rise to band ferromagnetism. This essentially is the consequence of the fact that an electron moves in the average field of the other electrons and ions; and the electron levels form energy bands. Due to a weak electron-electron interaction, an ordered magnetic state is stabilized and is characterized by different numbers of up and down spins.[6,7,10] Interestingly enough, presence of the magnetic ordering in iron, nickel, and cobalt leads to giant internal pressure and compressibility anomalies.[11] For instance, the magnetic $3d$ elements have a larger atomic volume than the trend of their neighbors.[3] Moreover, the measured volume and energy changes near the Curie temperature, T_C, are far smaller than would occur if the magnetic energy went to zero with bulk magnetization.[12] These discrepancies are reconciled by assuming the persistance of magnetic ordering at localized level in the paramagnetic state.[13,14] In fact, Korenman has shown that the local magnetization strength reduces by only a few percent at the Curie temperature.[15] The fact that the magnetism and the band structure of a ferromagnetic transition metal are related and since electrical resistivity can probe the electronic states, this technique is quite useful, especially under high pressure and high temperature, where other conventional techniques cannot be used.

II. STATEMENT OF THE PROBLEM

Electrical resistivity of nickel and iron is explained through the scattering of electrons by various sources such as phonons, magnons, other electrons and impurities. It is observed that in these metals electrical resistivity follows a T^2 dependence below the Curie temperature T_C, and a T dependence above the Curie temperture.[16,17] These are shown in Figs. 1 and 2 for nickel and iron, respectively.[18,19] A kink in the electrical resistivity can be noticed at the transition temperature T_C. Mott ascribed the change of slope in nickel mainly to the change in the Fermi surface on approaching the Curie temperature.[10]

The argument is as follows. At low temperature, conduction electrons with spins parallel to the direction of magnetization cannot make transitions to the d band, since the spin-up d band is full. Thus, these electrons (sp electrons with spinup) would have a much longer mean free path than those with opposite spin. However, as the temperature is raised, the s-d transition can occur for electrons with either spin directions. According to this model nickel above the Curie temperature should behave like Pd. In fact, it is found to be true, as depicted in Fig. 3. Mott, thus suggested that the scattering by spin disorder, though doubtless present, is not the only effect in
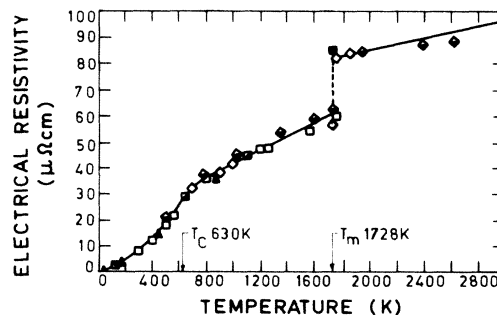
FIG. 1. Electrical resistivity ρ of nickel as a function of temperature. A T^2 dependence below T_C and a linear variation above T_C can be seen. That is, there is a change of slope at the magnetic transition temperature, $T_C = 630$ K. A discontinuity in ρ occurs due to melting at $T_m = 1728$ K.
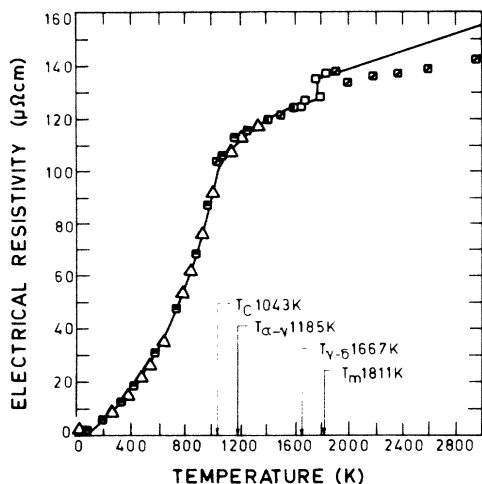
FIG. 2. Electrical resistivity of iron as a function of temperature. Similar behavior around T_C, as in nickel, is observed in this case also. Structural transitions α-γ, γ-δ, and solid-liquid transitions lead to discontinuous changes in ρ corresponding to the temperatures $T_{\alpha\text{-}\gamma} = 1185$ K, $T_{\gamma\text{-}\delta} = 1667$ K, and $T_m = 1811$ K.

nickel.[10] On the other hand, in Fe, scattering by spin disorder is expected to be more important than that arising due to the change in the Fermi surface when traversing the magnetic transition. The reasons are as follows: (i) In α-Fe, both spin-up and spin-down bands have Fermi surfaces, (ii) it is much more likely than for nickel that coupled spins persist above T_C, and (iii) the magnetic moments of each atom is large ($2.45\mu_B$/atom) as compared to that of nickel ($0.59\mu_B$/atom). Thus in iron, the spin-wave scattering should be larger than that in nickel. Mott, in the review article showed how the T^2-dependent resistivity will arise from spin-wave scattering and will have an equally important contribution from the asymmetry in the Fermi surface.[20] In addition, the T^2-dependent resistivity arising out of electron-magnon scattering saturates at T_C, while that due to the Baber

scattering, arising as a consequence of normal scattering of the "light" s electrons with the "heavy" d electrons (e_s, e_d scattering) is expected to contribute even above the Curie temperature.[10,21,22] According to Mott, only at fairly high temperatures, as the holes in the d band become nondegenerate, the contribution from the Baber scattering should flatten out.[23]

It would be instructive if the various effects could be distinguished experimentally. In this context, it is gratifying to mention that upon alloying nickel with a small amount of Pd, the increased resistance above the Curie temperature due to the greater effect of s-d scattering (through the band-structure effect) was demonstrated while traversing the Curie temperature.[24,25] However until recently no reasonable experimental evidence for the Fermi-surface change across the magnetic transition has been established.[15,26,27] Conventional techniques such as the de Haas—van Alphen effect, cyclotron resonance, and other oscillatory galvanomagnetic techniques cannot be used to map the Fermi surface at high temperatures such as T_C. For example, it is a prerequisite of the conventional quantum oscillatory measurements that the electrons should undergo a very large number of oscillations before these can get thermally scattered. In this context, the attempt by Stachowiak, and Kontrym-Sznajd et al. are worth mentioning.[28,29] By studying the angular correlation of annihilation quanta in a positron technique, they found that the Fermi surface of nickel in the ferromagnetic phase has a copperlike neck and that this neck becomes considerably diffuse in the paramagnetic phase. To the best of our knowledge, such a type of result on iron has not been reported so far.[30,31] In this paper we report high-pressure and high-temperature electrical resistivity measurements on nickel and iron and show in the subsequent sections that an alternative route to visualize the above problem is possible. The focal theme is the following. The pressure variation of the electrical resistivity ρ of a ferromagnetic transition metal is a strong function of the band structure.[32] If there is a Fermi surface change and hence a band structure change across the magnetic transition, $\partial \ln\rho / \partial P$ on either side of the magnetic transition temperature is expected to be different.

III. EXPERIMENTAL PROCEDURE

High-pressure, high-temperature electrical resistivity measurements were performed on 99.999% pure foils of nickel and iron procured from Johnson Mathey, England. The experimental technique, discussed in detail elsewhere,[33] enabled continuous pressure and temperature calibration of the high-pressure, high-temperature cell. The cell was confined in an opposed-anvil high-pressure device and had an internal heating arrangement. The pressure calibration[34] was done by following the phase diagram of Bi, Sb, etc. and the temperature was obtained using the Pt—(Pt-10 at. % Rh) thermocouple. Also, the appropriate pressure correction to the thermo-emf was done to get the exact cell temperature.[34]

All runs, in which the signal due to the temperature gradient led to thermo-emf more than 0.1% of the sample voltage, were rejected. The electrical resistivity could be
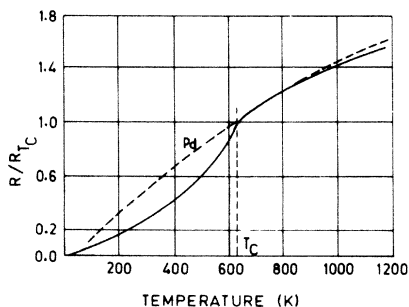
FIG. 3. Electrical resistance of nickel and palladium as a function of temperature. Below T_C, a T^2-dependent resistance variation in nickel is seen. Above T_C resistance of nickel varies as that of palladium (Ref. 16).
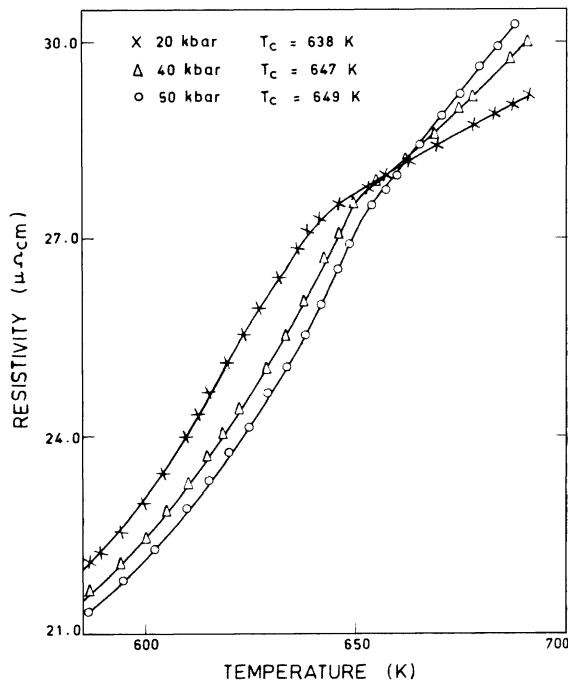
FIG. 4. High-pressure and high-temperature electrical resistivity of nickel. The reversal in the behavior of resistivity above T_C can be seen. The resistivity below T_C is normal, that is, ρ decreases with pressure. Above T_C, the behavior is anomalous and leads to a positive pressure coefficient of resistivity.

measured with a resolution of 1 in 10^6 and the quantity $\partial \ln\rho/\partial P$ had a resolution of 5 in 10^5. The quantity $\partial \ln\rho/\partial P$ was obtained using

$$\frac{\partial \ln\rho}{\partial P} = \frac{\partial \ln R}{\partial P} - \frac{K_T}{3} = \frac{\partial \ln V'}{\partial P} - \frac{K_T}{3} \qquad (1)$$

and the voltage output from the sample. The high-pressure and high-temperature electrical resistivity of nickel, as obtained from the raw data presented in Table I is depicted in Fig. 4. To bring out the features around T_C, only a range of temperatures 583—681 K is covered in Fig. 4. A change in the slope marks the transition (ferromagnetic→paramagnetic phase). Rough location of the Curie temperature is done by plotting $\partial\rho/\partial T$ as a function of temperature at various pressure, and finding the maximum in this quantity. Then, a detailed analysis,[35] given in Appendix A is used for the exact location of T_C. From the T_C values so obtained, $\partial T_C/\partial P$ is found to be 0.4 K kbar^{-1} which is in good agreement with the value of 0.38 K kbar^{-1} reported by Leger et al.[36]

The interesting part of the experiment, as can be visualized from Fig. 4, is the effect of pressure on the electrical resistivity below and above T_C. This can be appreciated more convincingly by discussing the relevant parameter, the pressure coefficient of electrical resistivity (PCR). For $T < T_C$, ρ decreases with pressure and PCR is -1.6×10^{-3} kbar^{-1} and is in close agreement with the value in literature.[37] However, for $T > T_C$, ρ increases

with pressure and the PCR is $+8.5\times10^{-4}$ kbar^{-1}. That is, there is a sign reversal in the PCR of nickel across the magnetic transition.

Similar experiments on iron were performed at 7 and 16 kbar respectively. The data are presented in Table II. The electrical resistivity extracted from the primary data

TABLE I. Primary data obtained under pressure P and temperature T for nickel.

T (K)[a]	Voltage output (μV)		
	P=20 kbar	P=40 kbar	P=50 kbar
583	229.80	226.03	224.13
588	232.55	229.18	227.04
591	234.70	231.10	228.72
595	237.68	233.70	231.33
598	239.75	235.38	232.86
602	243.42	238.82	236.07
605	246.94	241.89	239.13
609	250.92	245.41	242.35
611	253.36	247.10	243.88
618	260.54	254.51	250.91
621	263.22	256.63	253.61
622	265.00	257.81	254.49
623	265.89	259.31	256.07
625	268.03	261.09	258.09
628	270.10	263.21	260.19
630	272.22	265.01	261.74
632	274.60	267.11	263.80
633	275.50	268.33	265.03
634	277.33	269.80	266.50
636	279.70	271.61	268.45
637	280.90	273.45	270.42
639	282.11	275.52	272.53
641	283.03	278.21	274.66
643	283.61	279.44	276.13
644	283.92	280.61	277.58
645	284.35	281.81	278.54
646	285.12	283.00	280.33
648	285.55	284.51	281.50
649	286.30	285.40	283.92
651	287.22	286.66	285.44
653	287.50	287.21	286.61
654	288.15	288.19	288.10
657	288.40	289.00	289.31
658	289.31	289.61	290.18
660	289.56	290.50	291.51
662	290.35	292.45	293.50
664	290.95	293.50	294.70
666	291.41	294.25	296.20
667	292.60	295.91	297.85
669	293.20	296.31	299.41
671	293.65	296.95	300.34
674	294.55	298.45	301.80
675	295.34	299.05	302.69
677	295.89	299.95	303.22
678	296.22	300.75	305.80
679	296.75	301.05	306.01
681	297.75	301.91	306.77

[a]Temperature T (K) is an average over a large number of readings and the temperature stability of our set up is ±1 K.
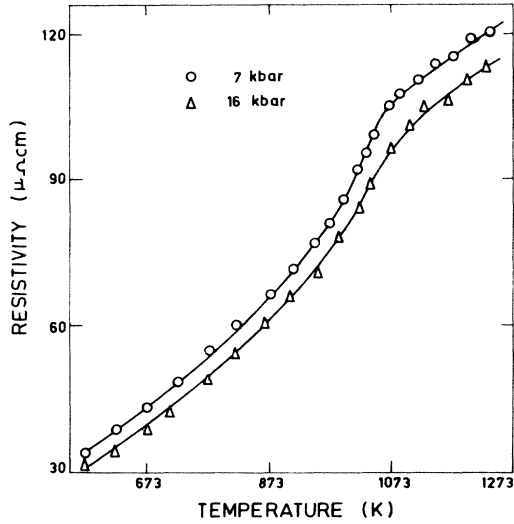
FIG. 5. High-pressure and high-temperature electrical resistivity of iron. The data taken at 7 and 16 kbar are shown. It is noticed that the pressure coefficient of resistivity is negative both above and below T_C.

is depicted in the Fig. 5.

T_C is located following the procedure as discussed for nickel and is found to be almost independent of pressure. This fact is in fair agreement with the data reported by Leger et al.[36] The value of $\partial T_c/\partial P$ reported by them is $\sim \pm 0.02$ K kbar^{-1}. The other feature worth mentioning is the normal behavior of the PCR. Its magnitude is -2.10×10^{-3} kbar^{-1} and is independent of temperature.

TABLE II. Primary data obtained under pressure and temperature for iron.

T (K)[a]	Voltage output (μV)	
	$P = 7$ kbar	$P = 16$ kbar
573	122.93	115.78
623	135.05	125.74
673	153.87	141.11
704	167.72	153.22
725	174.65	160.52
768	197.81	177.44
818	217.07	196.07
872	238.06	220.74
903	255.37	236.76
947	278.10	259.59
967	292.17	274.85
981	298.66	283.51
991	310.56	288.92
1013	333.29	302.99
1030	343.46	313.81
1035	357.09	331.15
1064	378.73	341.94
1084	387.39	354.28
1102	393.88	364.02
1116	399.94	371.16

[a]See footnote under Table I.

This value is in agreement with that in literature,[38] being -2.2×10^{-3} kbar^{-1}.

IV. ELECTRICAL RESISTIVITY OF A FERROMAGNETIC TRANSITION METAL

A variety of scattering processes contribute to the electrical resistivity of a ferromagnetic transition metal. The first of these and common to all the metals is due to the conduction (sp) electron-phonon scattering process, and is denoted by $\rho_{s\text{-}s}$. That part of conduction electron-phonon scattering in which the sp electrons are trapped into d states constitutes another process and is termed $\rho_{s\text{-}d}$, and it is larger than $\rho_{s\text{-}s}$ by a factor which is the ratio of the velocities of sp electrons to the d electrons.[39] For a magnetic transition metal, as a consequence of polarized d bands, the two-current model, as suggested by Mott, is operative,[32] i.e., $\rho_{s\text{-}d} = (\rho_{s\text{-}d}^{\uparrow}\rho_{s\text{-}d}^{\downarrow})/(\rho_{s\text{-}d}^{\uparrow} + \rho_{s\text{-}d}^{\downarrow})$. Normal electron-electron scattering also contributes significantly as shown by Ruthruff et al.[40] This is mainly due to the fact that during the direct scattering of "light" sp electrons by the "heavy" d electrons, the velocity conservation breaks.[41] This contribution is denoted by ρ_{e_s,e_d}. Finally, we consider the electron-magnon scattering process, a feature of the ferromagnetic transition metal. The contribution to resistivity from this process is termed as ρ_{mag}. Hence, the electrical resistivity of a pure ferromagnetic transition metal can be expressed as

$$\rho = \rho_{s\text{-}s} + \rho_{s\text{-}d} + \rho_{e_s,e_d} + \rho_{\text{mag}} . \tag{2}$$

An expression for the electrical resistivity of a transition metal due to electron-phonon interaction has been obtained by Grimvall[42] and is given as

$$\rho_{s\text{-}d} = \frac{3k_B}{\hbar e^2} V \frac{1}{N(E_F)} \frac{\lambda}{\langle v^2 \rangle_s} T . \tag{3}$$

Here V, $N(E_F)$, λ, and $\langle v^2 \rangle_s$ are the atomic volume, the total electron density of states at the Fermi level per atom, the electron mass enhancement factor,[43] and the expectation value of the square of the sp electrons velocity at the Fermi surface. By incorporating a two-current model, a requirement in a ferromagnetic transition metal, Eq. (3) is modified to read as

$$\rho_{s\text{-}d} = \frac{3k_B}{\hbar e^2} V \frac{[N^{\uparrow}(E_F) + N^{\downarrow}(E_F)]}{[N^{\uparrow}(E_F)N^{\downarrow}(E_F)]} \frac{\lambda}{\langle v^2 \rangle_s} T . \tag{4}$$

In Eq. (4), it is assumed that $v_s^{\uparrow} = v_s^{\downarrow}$, which is found to be almost true.[44] The high-temperature magnetic resistivity of nickel and iron has been calculated by Joynt[45] and the expression for $T > T_C$ is given as

$$\rho_{\text{mag}} = \frac{\pi\hbar |p|^2}{6e^2 m^2 \langle v^2 \rangle_s} \langle (\nabla \cdot \hat{\mathbf{M}})^2 \rangle V \frac{(N_s^{\uparrow}N_d^{\downarrow} + N_s^{\downarrow}N_d^{\uparrow})}{(N_s^{\uparrow} + N_s^{\downarrow})^2} , \tag{5}$$

where N is the electron density of states at the Fermi surface per atom per spin and the subscripts signify the electron character. For brevity we use s for sp electrons and E_F is dropped from the $N(E_F)$. $|p|$ is the momentum transfer during the electron-magnon scattering, $\langle (\nabla \cdot \hat{\mathbf{M}})^2 \rangle$ refers to the mean of the square of the spatial variation in

$\hat{M}$, the unit vector in the direction of the local magnetization, and m is the electron mass. Equation (5), as mentioned earlier, represents the magnetic resistivity at temperatures above T_C and in order to incorporate the temperature dependence of ρ_{mag} below T_C, we introduce an ordering factor $f(M)$ expressed as

$$f(M) = \frac{2\left[1+\frac{M}{M_0}\right]^\beta \left[1-\frac{M}{M_0}\right]^\beta}{\left[1+\frac{M}{M_0}\right]^\beta + \left[1-\frac{M}{M_0}\right]^\beta} . \tag{6}$$

The justification for the form of $f(M)$ as represented in Eq. (6), is given in Appendix B. In the limiting case of $T \rightarrow T_C$, it can be seen that $f(M) \rightarrow 1$. Thus, the modified ρ_{mag} which holds good for $T > T_C$ and as well as for $T < T_C$ can be written as

$$\rho_{mag} = \frac{\pi\hbar|p|^2}{6e^{2m^2}\langle v^2\rangle_s} \langle(\nabla\cdot\hat{M})^2\rangle \frac{(N_s^\uparrow N_d^\downarrow + N_s^\downarrow N_d^\uparrow)}{(N_s^\uparrow + N_s^\downarrow)^2} f(M) . \tag{7}$$

Kaveh and Wiser[22] have given an exhaustive review of the electron-electron scattering in metals and they indicate that it varies as T^2. Ziman[41] has obtained an explicit expression for it. According to him ρ_{e_s,e_d} can be expressed as (in units of Ω m)

$$\rho_{e_s,e_d} \approx 8.1\times10^{19}\left[\frac{\pi^2 e}{4}\right]^2 \frac{1}{v_s E_F} \frac{k_F}{q}\left[\frac{v_s}{v_d}-1\right]^2\left[\frac{k_B T}{E_F}\right]^2 . \tag{8}$$

Here, k_F, q, and v_d are the Fermi wave number, electron screening length, and the velocity of the d electrons, respectively. If we neglect ρ_{s-s} (which is at least an order of magnitude smaller[39] than ρ_{s-d}) and the resistivity contributions due to imperfections and impurities, then the resistivity of a ferromagnetic transition metal is given as (in units of Ω m)

$$\rho = \frac{3k_B}{\hbar e^2} V\frac{[N^\uparrow(E_F)+N^\downarrow(E_F)]}{[N^\uparrow(E_F)N^\downarrow(E_F)]} \frac{\lambda}{\langle v^2\rangle_s} T$$

$$+ \frac{\pi\hbar|p|^2}{6e^2m^2\langle v^2\rangle_s} \langle(\nabla\cdot\hat{M})^2\rangle V\frac{(N_s^\uparrow N_d^\downarrow + N_s^\downarrow N_d^\uparrow)}{(N_s^\uparrow + N_s^\downarrow)^2} f(M)$$

$$+ 8.1\times10^{19}\left[\frac{\pi^2 e}{4}\right]^2 \frac{1}{v_s E_F} \frac{k_F}{q}\left[\frac{v_s}{v_d}-1\right]^2\left[\frac{k_B T}{E_F}\right]^2 . \tag{9}$$

Next it remains to obtain an expression for the electrical resistivity which can be used for obtaining its behavior as a function of pressure and temperature. An exact expression for $\rho(P,T)$ does not exist, and hence we use the parametrization method. That is, we find the effect of pressure on the parameters entering into the expression for resistivity. The procedure is given in detail in Appendix C and the desired expression is

$$\rho(P,T) = \rho_{s-d}(0,T)\frac{V}{V_0}\frac{g(0)}{g(P)}\frac{\lambda(P)}{\lambda(0)}\frac{\langle v^2(0)\rangle_s}{\langle v^2(P)\rangle_s}$$

$$+ \rho_{mag}(0,T)\frac{V}{V_0}\frac{f(M,P)}{f(M,0)}\frac{\phi(M,P)}{\phi(M,0)}$$

$$+ \rho_{e_s,e_d}(0,T)\left[\frac{E_F(0)}{E_F(P)}\right]^3\left[\frac{v_d(0)}{v_d(P)}\right]^2\frac{v_s(P)}{v_s(0)} . \tag{10}$$

Having obtained the explicit form for the electrical resistivity as a function of pressure and temperature, now we set to analyze the experimental results obtained on nickel and iron. First the temperature dependence of ρ is analyzed and then its pressure and pressure-temperature dependences are taken up subsequently.

V. NICKEL

Electrical resistivity of nickel is calculated by substituting the values of various parameters listed in the Table III. The temperature-dependent resistivity is obtained to be

$$\rho = 6.972\times10^{-3}T + 20.654 f(M) + 9.362\times10^{-6}T^2 . \tag{11}$$

Using the magnetization data of Crangle and Goodman,[46] $f(M)$ is calculated and is given in Table IV (see Appendix B for details). Next ρ is calculated from Eq. (11) as a function of temperature and is listed in Table V. Further,
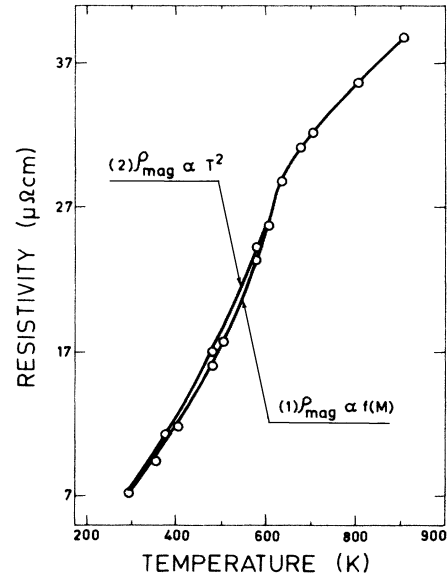
FIG. 6. Electrical resistivity of nickel as a function of temperature, where $\bigcirc$ represents experimental data. A change of slope occurs at 630 K. The continuous curve (1) represents the trend predicted by Eq. (11). Best fit with experimental data point requires that $\rho_{mag}(T)$ be made temperature dependent even above T_C. Plotted also is resistivity with $\rho_{mag} \propto T^2$ which can be noticed to overestimate the data points. (See Tables IV and V).

TABLE III. Values for the various parameters entering into the expression for electrical resistivity of nickel and iron.

Parameters[a]	Ni	Fe
V (m^3)	1.095×10^{-29}	1.182×10^{-29}
$N^\uparrow$ (states/J atom)	1.1839×10^{18}	5.9735×10^{18}
$N^\downarrow$ (states/J atom)	1.0052×10^{19}	1.3785×10^{18}
λ	0.67	0.29
$\mid p \mid$ (kg m s^{-1})	3.0×10^{-25}	4.1×0^{-25}
$\langle (\nabla \cdot \hat{\mathbf{M}})^2 \rangle$ (m^{-2})	$0.15 \times 10^{+20}$	$0.30 \times 10^{+20}$
m (kg)	1.289×10^{-30}	0.933×10^{-30}
$\langle v^2 \rangle_s$ (m^{2}s^{-2})	1.52×10^{12}	0.47×10^{12}
$f(M)$	See Tables IV and V	See Tables VIII and IX
$\langle v^2 \rangle_d$ (m^{2}s^{-2})	9.190×10^9	2.842×10^9
$N_s^\uparrow$ (states/J atom)	2.762×10^{17}	6.434×10^{17}
$N_s^\downarrow$ (states/J atom)	1.379×10^{17}	1.379×10^{17}
$N_d^\uparrow$ (states/J atom)	7.872×10^{17}	5.331×10^{18}
$N_d^\downarrow$ (states/J atom)	9.791×10^{18}	1.241×10^{18}

[a]All parameters evaluated at 1 atm.

the calculated values are plotted as a continuous curve (1) in Fig. 6, where the experimental points are also indicated in order to have a comparison. It is noticed that the fit is quite good for temperature up to T_C. In order to have good agreement between the experimental and calculated values above T_C, it is found essential that the magnetic resistivity be made temperature dependent. In fact, for 630 K < T < 900 K, the relation

$$\rho_{\text{mag}}(T) = \rho_{\text{mag}}(T_C)[1 + 8.1 \times 10^{-4}(T - T_c)]$$

or   (12)

$$\rho_{\text{mag}}(T) = 20.654[1 + 8.1 \times 10^{-4}(T - 630)]$$

is found to represent the experimental values adequately.[47] Also plotted in Fig. 6 as a continuous curve (2) is the $\rho_{\text{mag}} \propto (T/T_C)^2$. A comparison of curve (2) with experimental points indicates that curve (2) lies above the data points for $T < T_C$.

Now we turn to the high-pressure data analysis. Incorporating the pressure dependence of various factors in Eq. (10), the pressure- and temperature-dependent electrical resistivity of nickel can be written as (in units of $\mu \Omega$ cm)

$$\rho(P,T) = 6.972 \times 10^{-3} T \frac{V}{V_0} \frac{g(0)}{g(P)} \frac{\lambda(P)}{\lambda(0)} \frac{\langle v^2(0) \rangle_s}{\langle v^2(P) \rangle_s}$$

$$+ 20.654 \frac{V}{V_0} \frac{f(M,P)}{f(M,0)} \frac{\phi(M,P)}{\phi(M,0)}$$

$$+ 9.362 \times 10^{-6} T^2 \left[\frac{E_F(0)}{E_F(P)} \right]^3 \left[\frac{v_d(0)}{v_d(P)} \right]^2 \frac{v_s(P)}{v_s(0)}.$$

(13)

All the parameters are defined in Appendix C and the values of relevant parameters at relevant pressures are listed in the Tables VI and VII. Equation (13) is used to calculate the electrical resistivity at 293 K for nickel as a function of pressure and is depicted in Fig. 7 as a continuous curve. Also plotted in the Fig. 7 are the experimental points. The agreement obtained is quite close except in the pressure region near and above 40 kbar. This discrepancy may be due to the uncertainties in the values of the various parameters entering Eq. (13) and evaluated at high pressure. It now remains to calculate the resistivity of nickel as a function of temperature and at various fixed pressures. Using Eq. (13), the calculation has been

TABLE IV. Ordering parameter $f(M)$ is calculated for nickel at various temperatures along with $(T/T_C)^2$. Next, $\rho_{\text{mag}}(T < T_C)$ are calculated with $\rho_{\text{mag}}(T_C) = 20.654 \mu \Omega$ cm.

T (K)	$\dfrac{M}{M_0}$	$1 + \dfrac{M}{M_0}$	$1 - \dfrac{M}{M_0}$	$\left[1 + \dfrac{M}{M_0}\right]^{0.75}$ (I)	$\left[1 - \dfrac{M}{M_0}\right]^{0.75}$ (II)	$f(M) = \dfrac{2(\text{I})(\text{II})}{\text{I} + \text{II}}$	$\left[\dfrac{T}{T_c}\right]^2$ $T = 630$ K	$\rho_{mag} = 20.654$ ($\mu \Omega$ cm) $f(M)$	$(T/T_C)^2$
293	0.942	1.942	0.058	1.645	0.118	0.220	0.216	4.555	4.467
373	0.882	1.882	0.118	1.607	0.201	0.358	0.350	7.390	7.240
473	0.794	1.794	0.206	1.550	0.306	0.511	0.563	10.550	11.642
573	0.544	1.544	0.456	1.385	0.555	0.792	0.827	16.366	17.086
630	0	1	1	1	1	1	1	20.654	20.654

TABLE V. Resistivity of nickel is calculated for selected temperatures using the Eq. (11), that is, $\rho = 6.972 \times 10^{-3}T + 20.654f(M) + 9.362 \times 10^{-6} \ T^2$ (in units of $\mu \Omega$ cm). Also ρ is calculated by replacing $f(M)$ with $(T/T_C)^2$. The values are compared with experimental data, and are plotted in Fig. 6.

T (K)	$\rho_{s\text{-}d}$ ($\mu\Omega$ cm) I	$\rho_{\text{mag}} = 20.65$ ($\mu\Omega$ cm) $f(M)$ II	$\rho_{\text{mag}} = 20.65$ ($\mu\Omega$ cm) $(T/T_C)^2$ III	ρ_{e_s,e_d} ($\mu\Omega$ cm) IV	$\rho_{\text{calc},1}$ $= $ I + II + IV ($\mu\Omega$ cm)	$\rho_{\text{calc},2}$ $= $ I + III + IV ($\mu\Omega$ cm)	ρ_{obs} ($\mu\Omega$ cm)
293	2.043	4.544	4.467	0.804	7.390	7.314	6.93
373	2.600	7.394	7.240	1.303	11.297	11.143	10.50
473	3.298	10.554	11.642	2.094	15.946	17.035	15.90
573	3.995	16.358	17.086	3.074	23.427	24.154	23.10
630	4.392	20.654	20.654	3.716	28.762	28.762	28.90
700	4.880	20.654	20.654	4.587	30.122	30.122	32.34
800	5.578	20.654	20.654	5.992	32.223	32.223	35.80
850	5.926	20.654	20.654	6.764	33.344	33.344	37.37
900	6.275	20.654	20.654	7.583	34.512	34.512	38.95

done and the values are presented in Table VII. In Fig. 8, the calculated values of ρ at 50 kbar and as a function of temperature are shown as a continuous curve. Experimental data are also included therein. The experimental and calculated values are in good agreement for $T < T_C$. However, for $T > T_C$, a discrepancy can be noticed. The disagreement between the predicted and the observed trends becomes obvious if the pressure coefficient of electrical resistivity (PCR) is calculated. The PCR's predicted by Eq. (13) are negative at all temperatures, whereas in reality, there is a reversal in sign across the magnetic transition. Thus, since Eq. (13) does not reproduce even qualitatively the observed behavior of nickel, it is clear that a significant feature must be missing from the expression. Mott's conjecture on the band-structure change upon traversing the magnetic transition provides an elegant basis to resolve this discrepancy. The present work is believed to strengthen the findings of Kontrym-Sznajd et al.[29] on the change of the Fermi surface of nickel across the magnetic transition. It is gratifying to refer to

a growing body of the photoemission data and associated theoretical work which provide the evidence that electronic structure does change in nickel upon traversing the Curie temperature.[26,31,48−52]

VI. IRON

Electrical resistivity of iron is calculated by substituting the values of parameters listed in Table III. The temperature-dependent electrical resistivity is obtained to be (in units of $\mu \Omega$ cm)

$$\rho = 9.962 \times 10^{-3}T + 78.730f(M) + 1.302 \times 10^{-5}T^2 . \quad (14)$$

Using the magnetization data of Crangle and Goodman,[46] $f(M)$ is calculated and is given in Table VIII. Now, ρ is calculated from Eq. (14) as a function of temperature and listed in Table IX. Next, the calculated values are plotted as a continuous curve (1) in Fig. 9, where the experimental points are also indicated in order to make a comparison. It is noticed that the fit is quite good for temperatures up

TABLE VI. Pressure variation of various parameters entering into the expression for ρ.

P (kbar)	V (10^{-29} m^3)	λ	$N^\uparrow$ (Ry^{-1})	$N^\downarrow$ (Ry^{-1})	$\langle v^2 \rangle_s$ (10^{12} m^{2}s^{-2})	$\langle v^2 \rangle_d$ (10^{10} m^{2}s^{-2})	$N_s^\uparrow$ (Ry^{-1})	$N_s^\downarrow$ (Ry^{-1})	$N_d^\uparrow$ (Ry^{-1})	$N_d^\downarrow$ (Ry^{-1})	E_F (Ry)
					Nickel[a−d]						
0	1.095	0.670	2.576	21.873	1.520	0.919	0.601	0.300	1.713	21.305	0.694
20	1.090	0.656	2.557	21.589	1.542	0.926	0.581	0.296	1.724	21.026	0.699
40	1.075	0.643	2.538	21.305	1.543	0.934	0.560	0.293	1.734	20.746	0.706
50	1.072	0.636	2.529	21.162	1.549	0.985	0.550	0.291	1.740	20.607	0.709
					Iron[a,b,d,e]						
0	1.182	0.290	13.000	3.000	0.470	0.284	1.400	0.300	11.60	2.700	0.680
20	1.171	0.284	12.664	2.921	0.473	0.286	1.380	0.296	11.28	2.625	0.686
40	1.161	0.278	12.338	2.843	0.473	0.288	1.368	0.293	10.96	2.550	0.692
50	1.569	0.275	12.168	2.806	0.479	0.293	1.370	0.292	10.75	2.500	0.695

[a]S. N. Vaidya and G. C. Kennedy, J. Phys. Chem. Solids 31, 2329 (1970).
[b]Reference 1.
[c]Reference 34.
[d]Reference 35.
[e]Reference 16; also see V. K. Ratti, R. Evans, and B. L. Gyorffy, J. Phys. F 4, 371 (1974).

to T_C. It is, however, found necessary that ρ_{mag} be made temperature dependent, even above T_C, for a good agreement between the experimental and calculated values. For instance, for 1043 K $< T <$ 1185 K, the relation

$$\rho_{mag}(T) = \rho_{mag}(T_C)[1 + 8.173 \times 10^{-4}(T - T_C)]$$

or   (15)

$$\rho_{mag}(T) = 78.730[1 + 8.173 \times 10^{-4}(T - 1043)]$$

is found to give the calculated values of ρ in close agreement with the data points. As pointed out in Ref. 47 in the context of explaining high-temperature electrical resis-

tivity of nickel, it is satisfying to believe that the local moment persists even beyond the magnetic transition and decreases with the increase in temperature. This leads to an increase in the value of $\langle (\nabla \cdot \hat{\mathbf{M}})^2 \rangle$ and hence ρ_{mag} with the increase in temperature. In Fig. 8, also plotted is the curve (2) derived from $\rho_{mag}(T) \propto (T/T_C)^2$, which is seen to clearly overestimate the experimental points in the temperature region $T < T_C$.

Turning now to the high-pressure data analysis, by incorporating the pressure dependence of various factors in Eq. (10), the general form of the expression can be written for iron as (in units of $\mu \, \Omega \, cm$)

TABLE VII. Resistivity calculation for nickel under high pressure and high temperature using Eq. (13). Here pressure is varied from 1 atm to 50 kbar and temperature is varied from 293 to 900 K.

T (K)	$f(M,P)$	$\rho_{s\text{-}d}$ ($\mu \, \Omega \, cm$)	ρ_{mag} ($\mu \, \Omega \, cm$)	ρ_{e_s, e_d} ($\mu \, \Omega \, cm$)	ρ ($\mu \, \Omega \, cm$)	ρ [using Eq. (12)] ($\mu \, \Omega \, cm$)
			$P = 1$ atm			
293	0.220	2.043	4.544	0.804	7.391	7.391
373	0.355	2.601	7.232	1.302	11.239	11.239
473	0.571	3.298	10.550	2.094	15.947	15.947
573	0.792	3.995	16.350	3.073	23.427	23.427
630	1	4.392	20.654	3.716	28.770	28.770
700	1	4.881	20.654	4.588	30.122	31.293
800	1	5.580	20.654	5.991	32.224	35.088
850	1	5.926	20.654	6.760	33.350	36.863
900	1	6.275	20.654	7.583	34.513	39.030
			$P = 20$ kbar			
293	0.214	1.980	4.444	0.784	7.208	7.208
373	0.346	2.521	7.168	1.270	10.959	10.959
473	0.498	3.196	10.317	2.042	15.556	15.556
573	0.722	3.870	15.994	2.997	22.863	22.863
630	0.975	4.257	20.210	3.820	28.081	28.081
700	0.975	4.731	20.210	4.473	29.404	30.550
800	0.975	5.406	20.210	5.842	31.450	34.233
850	0.975	5.744	20.210	6.596	32.540	35.978
900	0.975	6.082	20.210	7.394	33.677	38.097
			$P = 40$ kbar			
293	0.209	1.928	4.306	0.756	6.991	6.991
373	0.337	2.454	6.948	1.226	10.630	10.630
473	0.485	3.110	10.000	1.972	15.086	15.086
573	0.752	3.770	15.500	2.894	22.166	22.166
630	0.950	4.155	19.572	3.498	27.216	27.216
700	0.950	4.606	19.572	4.318	28.497	29.607
800	0.950	5.264	19.572	5.640	30.477	33.177
850	0.950	5.593	19.572	6.367	31.533	34.862
900	0.950	5.922	19.570	7.139	32.63	36.910
			$P = 50$ kbar			
293	0.207	1.902	4.264	7.113	6.880	6.880
373	0.334	2.421	6.880	1.153	10.454	10.454
473	0.480	3.071	9.904	1.854	14.830	14.830
573	0.744	3.720	15.350	2.721	21.790	21.790
630	0.940	4.090	19.381	3.288	26.860	26.860
700	0.940	4.540	19.380	4.060	27.860	28.959
800	0.940	5.193	19.380	5.300	29.870	32.538
850	0.940	5.518	19.380	5.980	30.870	34.166
900	0.940	5.840	19.380	6.710	31.360	35.598
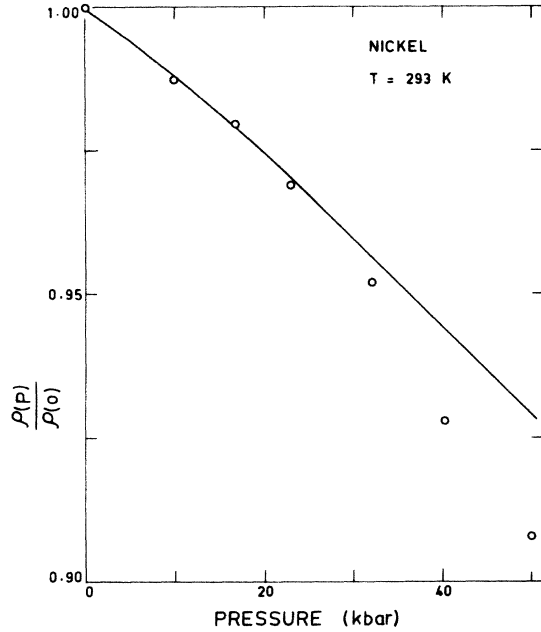
FIG. 7. Electrical resistivity of nickel as a function of pressure. O represents the data and the continuous curve is obtained from Eq. (13). The agreement between the calculated and experimental values is good except near 40 kbar and above. This may be due to the uncertainties in the various parameters figuring in Eq. (13) evaluated at high pressures.
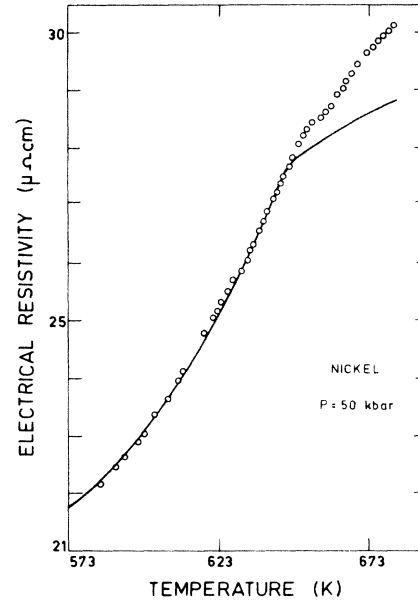
FIG. 8. Electrical resistivity of nickel as a function of temperature obtained at 50 kbar. Calculated values from Eq. (13) are also plotted as a continuous curve. It is noticed that for $T > 650$ K, experimental values are much larger than the values obtained from Eq. (13). This is because of the band-structure change across the magnetic transition.

$$\rho(P,T) = 9.962 \times 10^{-3} T \frac{V}{V_0} \frac{g(0)}{g(P)} \frac{\lambda(P)}{\lambda(0)} \frac{\langle v^2(P) \rangle_s}{\langle v^2(0) \rangle_s}$$

$$+ 78.730 \frac{V}{V_0} \frac{f(M,P)}{f(M,0)} \frac{\phi(M,P)}{\phi(M,0)}$$

$$+ 1.302 \times 10^{-5} T^2 \left[\frac{E_F(0)}{E_F(P)} \right]^3 \left[\frac{v_d(0)}{v_d(P)} \right]^2 \frac{v_s(P)}{v_s(0)} . \tag{16}$$

All the parameters are defined in Appendix C and the values of relevant parameters at relevant pressures are listed in Tables VI and X. Equation (16) is used to calculate the electrical resistivity at 293 K for iron as a function of pressure and is depicted in Fig. 10 as a continuous curve. Also plotted in Fig. 10 are the experimental points. It is noted that agreement is quite close except in the pressure region near 40 kbar and above. The calculated values are also listed in Tables X and XI. In Fig. 11, the calculated values of ρ at the pressure of 16 kbar and as a function of

TABLE VIII. Ordering parameter $f(M)$ is calculated for iron at various temperatures along with $(T/T_C)^2$. It is found necessary to vary β with temperature in order to have reasonable agreement with experimental data, shown in Fig. 9. $\rho_{mag}(T_C)$ is set at 78.730 $\mu \Omega$ cm.

T (K)	$\dfrac{M}{M_0}$	$1+\dfrac{M}{M_0}$	$1-\dfrac{M}{M_0}$	β	$\left\|1+\dfrac{M}{M_0}\right\|^{\beta}$ (I)	$\left\|1-\dfrac{M}{M_0}\right\|^{\beta}$ (II)	$f(M)=\dfrac{2(I)(II)}{I+II}$	$\left\|\dfrac{T}{T_C}\right\|^2$ (T_C=1043 K)	ρ_{mag}=78.730 ($\mu \Omega$ cm) $f(M)$	$(T/T_C)^2$
293	0.981	1.981	0.019	0.83	1.764	0.037	0.073	0.079	5.747	6.213
300	0.981	1.981	0.019	0.82	1.752	0.039	0.076	0.083	5.974	6.513
400	0.968	1.968	0.032	0.79	1.707	0.066	0.127	0.147	9.995	11.579
500	0.947	1.947	0.053	0.76	1.660	0.107	0.201	0.230	15.864	18.093
600	0.916	1.916	0.084	0.74	1.618	0.160	0.291	0.331	22.920	26.054
700	0.875	1.875	0.125	0.71	1.562	0.229	0.399	0.450	31.384	35.462
800	0.810	1.810	0.190	0.70	1.515	0.312	0.518	0.588	40.813	46.318
900	0.715	1.715	0.285	0.60	1.382	0.471	0.702	0.744	55.303	58.621
1000	0.495	1.495	0.505	0.60	1.272	0.664	0.872	0.919	68.690	72.372
1043	0	1	1		1	1	1	1	78.730	78.730

temperature are plotted as a continuous curve. In order to have an idea of the comparison, the data points are also included in the Fig. 11. It is noticed that the data points fall nicely on the calculated values.

VII. DISCUSSION

In a Heisenberg ferromagnet, the magnetic and electronic degrees of freedom are treated separately, for, the latter does not contribute to the thermodynamics of the magnetism as they are frozen out. On the contrary, in the case of an itinerant ferromagnet, there is an interplay between the changes of the electronic structure and magnetism.[53-62] This interplay is expected to be quite prominent at the magnetic transition. For instance, in the Stoner model of ferromagnetism, below T_C, there are spin-polarized energy bands which get unpolarized across the magnetic transition. Controversy over the fact that spin-wave-like modes are present even above T_C has led to further interest in the magnetism of the itinerant ferromagnets such as nickel and iron.[63-67] However, the undisputable conclusion that has been arrived at, from a large number of experiments, and is consistent with the prediction of Oguchi is that the exchange energy splitting decreases with temperature.[68,69] Moreover, the decrease in the exchange energy splitting is not as fast as demanded by the Stoner model.[49] This is shown in the Fig. 12, where the variation in exchange energy splitting δE_{ex}, as observed in photoemission experiment,[48] is plotted along with the variation in the bulk magnetization, M_s. Also plotted is the theoretical curve of Oguchi.[69]

In continuation of the above, it is worth mentioning the recent spin-polarized photoemission results by Hopster et al.[51] They found that the exchange energy split peaks measured at the X point of the energy bands of the nickel are observed to merge and broaden as the temperature rises through T_C. Local band theory calculation based on the temperature-independent mean-field strength and the
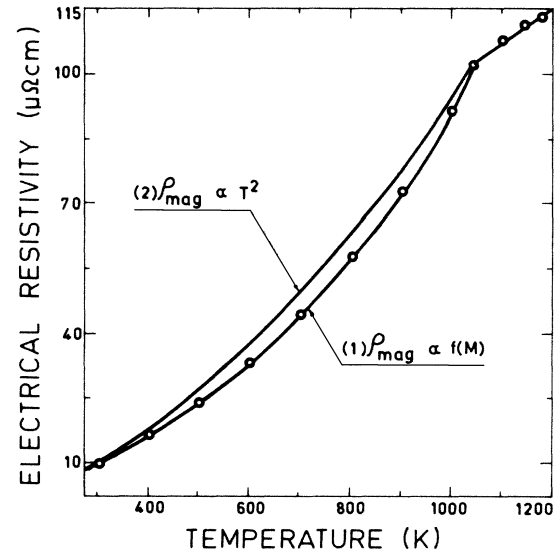
FIG. 9. Electrical resistivity of iron as a function of temperature where O represents experimental data. A change of slope at 1043 K can be noticed. The continuous curve (1) represents the trend predicted by Eq. (14). A better fit in the range of temperatures 1043 to 1185 K requires $\rho_{mag}(T) = \rho_{mag}(T_C)$ $[1 + 8.173 \times 10^{-4}(T - T_C)]$. Also, $\rho_{mag} = \rho_{mag}(T_C)$. $(T/T_C)^2$ is seen to overestimate the data points. The details can be found in Tables VIII and IX.

temperature dependent ordering scale predicts that the intrinsic spectrum changes the splitting only by $\sim 30\%$ at the X point of the polarized energy bands. Thus, the general consensus, at the moment, centers on the idea that the long-range magnetic order exists up to the Curie temperature; and above T_C, the short-range magnetic order persists. Furthermore, the short-range magnetic order decreases with temperature as is evident from the curves (1)

TABLE IX. Resistivity of iron is calculated for selected temperatures using Eq. (14); that is, $\rho = (9.962 \times 10^{-3})T + 78.730 f(M) + (1.302 \times 10^{-5})T^2$ (in units of $\mu\,\Omega\,cm$). Also ρ is calculated by replacing $f(M)$ with $(T/T_C)^2$. The values are compared with the observed data. This comparison is done in Fig. 9 also.

T (K)	$\rho_{s\text{-}d}$ ($\mu\,\Omega\,cm$)	$\rho_{mag} = 78.730$ ($\mu\,\Omega\,cm$) $f(M)$ II	$\rho_{mag} = 78.730$ ($\mu\,\Omega\,cm$) $(T/T_C)^2$ III	ρ_{e_s,e_d} IV ($\mu\,\Omega\,cm$)	$\rho_{calc,1}$ I + II + IV ($\mu\,\Omega\,cm$)	$\rho_{calc,2}$ I + III + IV ($\mu\,\Omega\,cm$)	ρ_{obs} ($\mu\,\Omega\,cm$)
293	2.919	5.747	6.213	1.118	9.784	10.250	9.61
300	2.989	5.983	6.513	1.172	10.144	10.673	9.98
400	3.985	9.999	11.579	2.083	16.067	17.647	16.10
500	4.981	15.824	18.093	3.255	24.060	26.329	23.72
600	5.977	22.910	26.054	4.687	33.575	36.718	33.06
700	6.973	31.413	35.462	6.380	44.766	48.815	44.27
800	7.970	40.782	46.318	8.333	57.084	62.620	57.56
900	8.966	55.268	58.621	10.546	74.780	78.133	73.11
1000	9.962	68.653	73.372	13.022	91.635	95.354	91.76
1043	10.390	78.730	78.730	14.164	103.284	103.284	102.20
1100	10.958	78.730	78.730	15.754	105.442	105.442	108.30
1150	11.456	78.730	78.730	17.219	107.405	107.405	111.50
1185	11.805	78.730	78.730	18.283	108.818	108.818	113.40
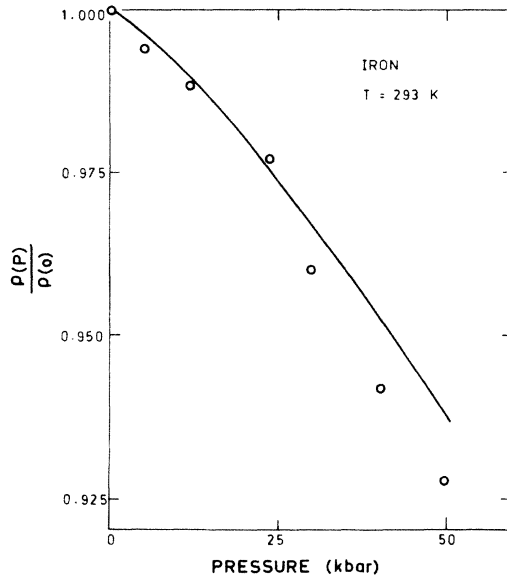
FIG. 10. Electrical resistivity of iron as a function of pressure. O represents the data point and the continuous curve is obtained from Eq. (16). Agreement between the calculated and experimental values is good except near 40 kbar and above. This may be due to the uncertainties in the various parameters figuring in Eq. (16) evaluated at high pressures.

and (4) in Fig. 12. It is interesting to recall the analysis of our data and their presentation in Figs. 6 and 9 which bear the fact that for the temperature above T_C, the ρ_{mag} should continue to show temperature dependence.[47] Turning now to the crucial part of our results, namely, the high-pressure and high-temperature electrical resistivity behavior of nickel and iron, in what follows, we have attempted to provide a plausible explanation.[70] In the paramagnetic phase of nickel, the situation can be described as follows.

(i) The spins are relatively free, that is, the spin-spin coupling is fairly weak; and the magnetic moments are comparatively localized.

(ii) During the electron-ion scattering, spin flip is possible.

(iii) The strength of this spin-flip scattering depends on the magnitude of the exchange splitting energy δE_{ex}.

TABLE X. Electrical resistivity variation of iron as a function of pressure and at 293 K.

P (kbar)	$\rho_{s\text{-}d}$ ($\mu\,\Omega$ cm)	ρ_{mag} ($\mu\,\Omega$ cm)	ρ_{e_s,e_d} ($\mu\,\Omega$ cm)	ρ ($\mu\,\Omega$ cm)
0	2.919	5.747	1.118	9.784
7	2.908	5.694	1.108	9.710
16	2.892	5.629	1.093	9.613
20	2.889	5.598	1.085	9.573
40	2.860	5.453	1.055	9.368
50	2.844	5.373	1.039	9.255
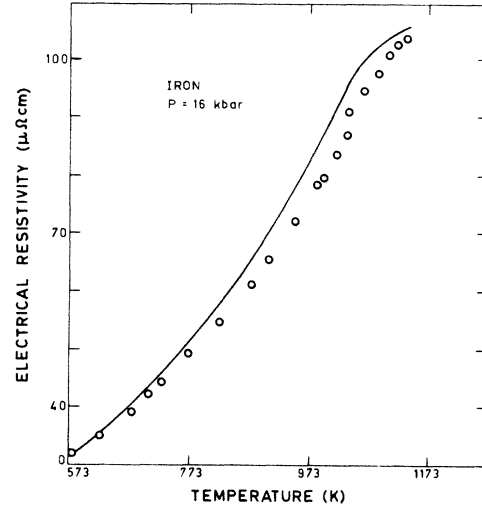
FIG. 11. Electrical resistivity of iron as a function of temperature at 16 kbar. Calculated values from Eq. (16) are also plotted as continuous curve. The agreement is quite good.

With the above, the scattering cross section per magnetic spin in the paramagnetic phase can be expressed as[71–73]

$$\Sigma = (4\pi)^{-1} \left[\frac{mJ}{\hbar^2} \right]^2 s(s+1) \,, \tag{17}$$

where J is the exchange interaction term, appearing in the interaction of a conduction electron with the ion. That is,

$$\mathcal{H}_{el\text{-}ion} = \mathcal{H}_{s\text{-}d} = -J \sum_{\sigma,\sigma'} \hat{S}_i s_{\sigma,\sigma'} \,. \tag{18}$$

Here $\hat{S}_i$ is the spin of the d electron from which the incoming conduction electron of spin σ is scattered such that its final spin is σ'. Moreover, in the realistic situation, the "heavy" d electrons are not strictly localized, thus, the scattering represented by Eq. (17) is essentially

TABLE XI. Electrical resistivity of iron as a function of temperature and pressure.

T (K)	ρ ($\mu\,\Omega$ cm)		
	$P=1$ atm	$P=7$ kbar	$P=16$ kbar
293	9.783	9.710	9.613
300	10.144	10.007	9.967
400	16.067	15.942	15.777
500	24.060	23.868	23.616
600	33.578	33.300	32.942
700	44.766	44.395	43.912
800	57.084	56.605	55.984
900	74.780	74.144	73.323
1000	91.635	90.849	89.836
1043	103.284	102.394	101.249
1100	105.442	104.536	103.366
1150	107.405	106.484	105.291
1185	108.818	107.886	106.677
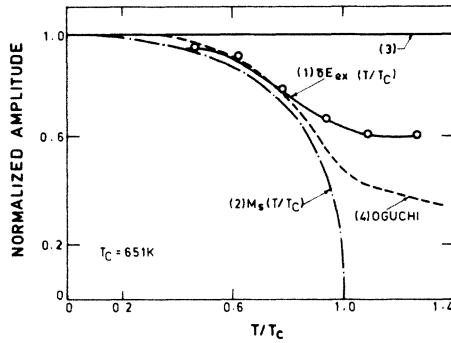
FIG. 12. Exchange-splitting in nickel is plotted as a function of temperature. Curve (1) refers to variation in the exchange-splitting as observed by Eastman and co-workers (Refs. 47 and 48). This data is compared with the variation in bulk magnetization curve (2), the temperature independent exchange splitting curve (3), and the calculation by Oguchi (Refs. 47, 49, 68, and 69).

an exchange version of Baber mechanism in which the exchange scattering of "light" electrons on the heavier electrons conserves the momentum but not the current and thus contributes to the electrical resistivity. Now, since the short-range exchange interaction overlap of wave functions is expected to increase with pressure, the resistivity should have an enhancement under pressure. This is precisely the situation in the paramagnetic nickel under pressure.

Moving to the pressure results on paramagnetic iron, we notice that, since δE_{ex} is quite large, spin flip scattering is not a dominant contribution. The usual processes operate which lead normally to a decrease in resistivity and hence, it is possible to explain the negative pressure coefficient of resistivity in paramagnetic phase. Considering another aspect, namely, the variation of $\partial \rho / \partial T$ with pressure, it is seen from Fig. 13 that in nickel, there is a large increase in its value as the pressure increases from

20 to 50 kbar. In fact, $\partial \rho / \partial T$ almost doubles in this pressure range. Moreover, there is a decrease in the value of $\partial \rho / \partial T$ in the range of atmospheric pressure to 20 kbar. Thus, there is a minimum in $\partial \rho / \partial T$ at ~ 20 kbar.[74]

We recall that in nickel there is a second-order transition at ~ 20 kbar.[75] For instance, Bastide and Loriers-Susse[75] found that for nickel, there is a discontinuity in the pressure coefficient of specific heat near 26 kbar suggesting the existence of a second-order transition. Interestingly enough, they found that the pressure dependence of the specific heat below and above T_C showed a marked difference and they believed that the transition is connected to the band structure of nickel. If that is the situation, then it is possible to explain the results shown in Fig. 13. That is, the change in the band structure around 20 kbar is the origin for the difference in the variation of $\partial \rho / \partial T$ in the two pressure ranges, namely, atmospheric pressure up to 20 kbar, and 20 to 50 kbar.

VIII. CONCLUSIONS

In an effort to understand the electrical behavior of nickel and iron under pressure and temperature it is noted that:

(i) The pressure coefficient of electrical resistivity of nickel changes sign and magnitude while traversing T_C.

(ii) The pressure coefficient of resistivity of iron is normal and is almost independent of temperature.

(iii) A minimum in $\partial \rho / \partial T$ is observed in nickel at 20 kbar which is connected to a second-order transition caused by the band-structure change.

(iv) Invoking the idea of exchange version of Baber scattering operative in paramagnetic nickel, it is possible to explain the increase in the electrical resistivity with pressure.

APPENDIX A: PROCEDURE FOR LOCATING T_C

Because of the spatial inhomogeneity and defects in the sample, the phase transition at $T = T_C$ becomes indistinct in the sense that it truncates the singularities of all quantities at T_C. Recently Kallback et al.[76] proposed that one of the reasons for rounding off is due to the critical slowing down at T_C as shown by the drift in the observed value. Due to this rounding off, T_C as determined from the position of the peak in the $\partial \rho / \partial T$ versus T curve may not be exact.[77]

In order to obtain the true value of T_C, we use scaling relation which states that $\alpha^+ = \alpha^-$, where α^+ and α^- are the critical exponents at $T \to T_C^+$ and $T \to T_C^-$, respectively. This approach was first used by Kollie[78] while extracting T_C of nickel by thermal expansion experiments. The critical exponents in the present case have been obtained by using the relation

FIG. 13. $\partial \rho / \partial T$ is plotted as a function of pressure at 670 K. Important feature to be noted is the increase in $\partial \rho / \partial T$ with pressure. The calculated values are always smaller. Also $\partial \rho / \partial T$ at 1 atm is larger than that at 20 kbar. This is possibly due to a second-order transition near 20 kbar.
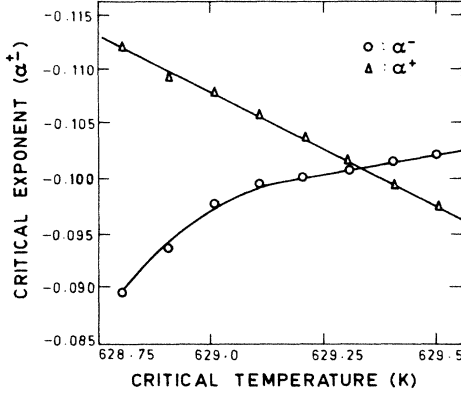
FIG. 14. Critical exponents as a function of T_C. The α^+ and α^- curves intersect at $\alpha^+ = \alpha^- = -0.101 \pm 0.006$, which gives the correct value of critical temperature, $T_C = 629.325$ K.

$$\frac{\partial \rho^{\pm}}{\partial T} = \frac{A^{\pm}}{\alpha^{\pm}} t^{-\alpha^{\pm}}(1 + Et^{+X^{\pm}}) + B \ . \tag{A1}$$

Here $t = |T/T_C - 1|$, " + " refers to $T \to T_C^+$, and "−" refers to $T \to T_C^-$. A is the critical amplitude and E is the measure of the amplitude correction terms. α is the leading critical exponent and X is the correction term arising as a consequence of confluent singularity. Using Eq. (A1) α^+ and α^- are obtained for a particular T_C. Now a new T_C is defined as $T_C + 0.1$ K and corresponding values of α^+ and α^- are obtained. Continuing this process, that is, by varying T_C at the step of 0.1 K, a large number of α^+ and α^- are obtained. Now α^+ and α^- are plotted as a function of T_C. At the point where α^+ and α^- curves intersect, $\alpha^+ = \alpha^-$, and the value of T_C so found is assigned to be the true critical temperature. In Fig. 14, the plot is shown where T_C was varied from 628.8 to 629.5 K in steps of 0.1 K. The critical exponent thus obtained is $\alpha^+ = \alpha^- = 0.101 \pm 0.006$ and the Curie temperature $T_C = 629.325$ K.

APPENDIX B: ORDERING FACTOR $f(M)$

The existence of short-range magnetic ordering above T_C is now an established fact.[47] Resistivity which is the measure of the disorder saturates at T_C and is given as

$$\rho_{\text{mag}} = \frac{\pi\hbar|p|^2 V\langle(\nabla\cdot\hat{\mathbf{M}})^2\rangle}{6e^2m^2\langle v^2\rangle_s} \frac{(N_s^\uparrow N_d^\downarrow + N_s^\downarrow N_d^\uparrow)}{(N_s^\uparrow + N_s^\downarrow)^2} \ . \tag{B1}$$

The fact that long-range order initiates as T decreases below T_C, we can multiply ρ_{mag} by an ordering parameter $f(M)$. According to Ziman,[39] in a parabolic band, this ordering parameter for spin-up and spin-down electrons are proportional to $(1 - M/M_0)^{1/3}$ and $(1 + M/M_0)^{-1/3}$, respectively. This in view of the two-current model will have the effective value of

$$2 \frac{\left[1 - \dfrac{M}{M_0}\right]^{1/3}\left[1 + \dfrac{M}{M_0}\right]^{1/3}}{\left[1 - \dfrac{M}{M_0}\right]^{1/3} + \left[1 + \dfrac{M}{M_0}\right]^{1/3}} \ . \tag{B2}$$

However, in the cases of nickel and iron, parabolic band approximation does not seem to give good agreement with the experimental values. As can be seen from Tables IV, V, VIII, and IX, $\beta = 0.75$ for nickel and $\beta = 0.83$–0.6 for iron give good agreement. In this way, the $f(M)$ is defined as

$$f(M) = 2\frac{\left[1 + \dfrac{M}{M_0}\right]^{\beta}\left[1 - \dfrac{M}{M_0}\right]^{\beta}}{\left[1 + \dfrac{M}{M_0}\right]^{\beta} + \left[1 - \dfrac{M}{M_0}\right]^{\beta}}$$

as used in Eq. (5).

APPENDIX C: EXPRESSION FOR $\rho(P,T)$

Electrical resistivity of a ferromagnetic transition metal is given as (in units of Ω cm)

$$\rho = \frac{3Vk_B}{\hbar e^2}\frac{1}{\{N^\uparrow(E_F)N^\downarrow(E_F)/[N^\uparrow(E_F) + N^\downarrow(E_F)]\}}\frac{T\lambda}{\langle v^2\rangle_s}$$

$$+ \frac{\pi\hbar|p|^2 V\langle(\nabla\cdot\hat{\mathbf{M}})^2\rangle}{6e^2m^2\langle v^2\rangle_s}$$

$$\times \frac{N_s^\uparrow(E_F)N_d^\downarrow(E_F) + N_s^\downarrow(E_F)N_d^\uparrow(E_F)}{[N_s^\uparrow(E_F) + N_s^\downarrow(E_F)]^2}f(M)$$

$$+ 8.1 \times 10^{19}\left[\frac{\pi}{2}\right]^4\frac{e^2}{v_s E_F}\left[\frac{v_s}{v_d} - 1\right]^2\left[\frac{k_B T}{E_F}\right]^2 \ , \tag{C1}$$

$$f(M) = 2\frac{\left[1 + \dfrac{M}{M_0}\right]^{\beta}\left[1 - \dfrac{M}{M_0}\right]^{\beta}}{\left[1 + \dfrac{M}{M_0}\right]^{\beta} + \left[1 + \dfrac{M}{M_0}\right]^{\beta}} \ , \tag{C2}$$

where β is a temperature-dependent function. Equation (C2) is used to obtain temperature-dependent electrical resistivity of the ferromagnetic transition metal. Pressure dependence of electrical resistivity is arrived at by considering the pressure variation of the factors contributing to it. For the sake of convenience, henceforth we shall write $N(E_F)$ simply as N. Let us look at the expression for resistivity term by term

$$\rho_{s\text{-}d}(P,T) = \frac{3k_B TV}{\hbar e^2}\frac{N^\uparrow(P) + N^\downarrow(P)}{N^\uparrow(P)N^\downarrow(P)}\frac{\lambda(P)}{\langle v^2(P)\rangle_s} \ . \tag{C3}$$

If we define

$$g(P) = \frac{N^\uparrow(P)N^\downarrow(P)}{N^\uparrow(P) + N^\downarrow(P)} \tag{C4}$$

then, $g(P)/g(0)$ is a measure of the change in g under pressure. Hence, it is easily noticed that

$$\rho_{s\text{-}d}(P,T)=\rho_{s\text{-}d}(0,T)\frac{V}{V_0}\frac{g(0)}{g(P)}\frac{\lambda(P)}{\lambda(0)}\frac{\langle v^2(0)\rangle_s}{\langle v^2(P)\rangle_s} \quad (C5)$$

Now, let us consider the second term and make the following assumptions.

(i) Pressure variations of $|p|^2$ and $m^2\langle v^2\rangle_s$ are similar such that the quantity $|p|^2/m^2\langle v^2\rangle_s$ is constant under pressure.

(ii) Short-range order parameter $\langle(\nabla\cdot\hat{\mathbf{M}})^2\rangle$ is constant for $T<T_C$ under pressure. In fact, any change in the magnetization is buried in the variation of $f(M)$.

Let us now define

$$\phi(M,P)=\frac{N_s^{\uparrow}(P)N_d^{\downarrow}(P)+N_s^{\downarrow}(P)N_d^{\uparrow}(P)}{[N_s^{\uparrow}(P)+N_s^{\downarrow}(P)]^2} \quad (C6)$$

and

$$f(M,P)=f(M,0)\left[\frac{T_C(0)}{T_C(P)}\right]^2. \quad (C7)$$

Equation (C6) is justified by recalling the fact that the electron magnon scattering varies as T^2 (even though, it leads to an overestimation) and it would be reduced if T_C increases. This is analogous to the fact that the Debye temperature increases with pressure and the electron pho-

non coupling is reduced. Using the definitions given in Eqs. (C2) and (C6), $\rho_{\text{mag}}(P,T)$ is given as

$$\rho_{\text{mag}}(P,T)=\rho_{\text{mag}}(0,T)\frac{V}{V_0}\frac{f(M,P)}{f(M,0)}\frac{\phi(M,P)}{\phi(M,0)}. \quad (C8)$$

Finally the expression for the ρ_{e_s,e_d} is obtained. Using the fact that $v_s\gg v_d$, $v_s/v_d-1\approx v_s/v_d$; and $q\approx k_F$, it can easily be seen that

$$\rho_{e_s,e_d}(P,T)=\rho_{e_s,e_d}(0,T)\left[\frac{E_F(0)}{E_F(P)}\right]^3\left[\frac{v_d(0)}{v_d(P)}\right]^2\frac{v_s(P)}{v_s(0)}. \quad (C9)$$

Combining Eqs. (C5), (C8), and (C9) we have

$$\rho(P,T)=\rho_{s\text{-}d}(0,T)\frac{V}{V_0}\frac{g(0)}{g(P)}\frac{\lambda(P)}{\lambda(0)}\frac{\langle v^2(0)\rangle_s}{\langle v^2(P)\rangle_s}$$

$$+\rho_{\text{mag}}(0,T)\frac{V}{V_0}\frac{f(M,P)}{f(M,0)}\frac{\phi(M,P)}{\phi(M,0)}$$

$$+\rho_{e_s,e_d}(0,T)\left[\frac{E_F(0)}{E_F(P)}\right]^3\left[\frac{v_d(0)}{v_d(P)}\right]^2\frac{v_s(P)}{v_s(0)}. \quad (C10)$$

[1]J. R. Anderson, D. A. Papaconstantopoulos, L. L. Boyer, and J. E. Schirber, Phys. Rev. B **20**, 3172 (1979).

[2]J. Callaway, in *Physics of Transition Metals 1980*, edited by P. Rhodes (IOP, London, 1980), p. 1.

[3]V. L. Moruzzi, J. F. Janak, and A. R. Williams, *Calculated Electronic Properties of Metals* (Pergamon, New York, 1978).

[4]J. F. Janak, Phys. Rev. B **20**, 2206 (1979).

[5]According to density-of-state decomposition, even a small fraction of f-like states are found to exist. For instance, in nickel, based on von Barth—Hedin prescription, the density of states for electrons of various characters are: $N_s^{\uparrow}(E_F)=0.1913$, $N_s^{\downarrow}(E_F)=0.4098$, $N_d^{\uparrow}(E_F)=1.713$, and $N_d^{\downarrow}(E_F)=0.0074$. All are expressed in (Ry spin)$^{-1}$ (Ref. 1).

[6]J. Friedel and C. M. Sayers, J. Phys. (Paris) **38**, 697 (1977).

[7]N. F. Mott and H. Jones, *The Theory of the Properties of Metals and Alloys* (Dover, New York, 1958), p. 189.

[8]F. Gautier, in *Magnetism of Metals and Alloys*, edited by M. Cyrot (North-Holland, Amsterdam, 1982), p. 1.

[9]For example, in nickel the d-band width measured between X_5 and X_2 is found to be more than 4 eV and is of the same general magnitude as the intra-atomic Coulomb energy.

[10]N. F. Mott, Adv. Phys. **13**, 325 (1964).

[11]J. F. Janak and A. R. Williams, Phys. Rev. B **14**, 4199 (1984).

[12]A. J. Holden, V. Heine, and J. H. Samson, J. Phys. F **14**, 1005 (1984).

[13]T. Moriya, in *Electron Correlation and Magnetism in Narrow Band Systems*, edited by T. Moriya (Springer-Verlag, Berlin, 1981), p. 2.

[14]R. E. Prange, in *Electron Correlation and Magnetism in Narrow Band Systems*, edited by T. Moriya (Springer-Verlag, Berlin, 1981), p. 63.

[15]V. Korenman, J. Appl. Phys. **57**, 3000 (1985).

[16]B. R. Coles, Adv. Phys. **7**, 40 (1958).

[17]R. J. Weiss and A. S. Morrotta, J. Phys. Chem. Solids **9**, 302 (1959).

[18]T. K. Chu and T. C. Chi, in *Properties of Selected Ferrous Alloying Elements*, Vol. III-1 of *McGraw-Hill/CINDAS Data Series on Materials Properties*, edited by Y. S. Touloukian and C. Y. Ho (McGraw-Hill, New York, 1981), p. 209.

[19]T. K. Chu and T. C. Chi, in *Properties of Selected Ferrous Alloying Elements*, Vol. III-1 of *McGraw-Hill/CINDAS Data Series on Materials Properties*, Ref. 18, p. 126.

[20]Using the analogy with resistivity arising due to electron-phonon scattering, Mott used the form $\rho\sim\int I(\theta)(1-\cos\theta)2\sin\theta\,d\theta$ to be valid for electron-magnon scattering. Using $\theta_{\max}=q_{\max}/k_F\propto T^{1/2}/k_F$, recalling that the term $(1-\cos\theta)$ is absent in the electron-magnon scattering process (as it does not involve the creation or annihilation of magnons), and using the fact that the probability $I(\theta)$ that an electron is scattered in a unit volume through angle θ varies as T, we have $\rho_{\text{mag}}\propto T^2$.

[21]A. H. McDonald and M. J. Laubitz, Phys. Rev. B **21**, 2638 (1980).

[22]M. Kaveh and N. Wiser, Adv. Phys. **33**, 257 (1984).

[23]N. F. Mott, Adv. Phys. **13**, 405 (1964).

[24]N. F. Mott, Adv. Phys. **13**, 411 (1964).

[25]B. R. Coles, Adv. Phys. **7**, 63 (1958).

[26]V. Korenman and R. E. Prange, Phys. Rev. Lett. **53**, 187 (1984).

[27]E. Kisker, J. Magn. Magn. Mater. **45**, 23 (1984).

[28]H. Stachowiak, in *Magnetism in Metals and Metallic Compounds*, edited by J. T. Lopuszanski, A. Pekatski, and J. Przystawa (Plenum, New York, 1973), p. 177.

[29]G. Kontrym-Sznajd, H. Stachowiak, W. Wierzchowski, K. Petersen, N. Thrane, and G. Trumpy, Appl. Phys. **8**, 151 (1975).

[30]The Curie temperature of iron is 1043 K and hence performing high-temperature experiments to study the Fermi surface through a conventional techniques is a tedious task. However, the angle-resolved photoemission experiment done recently by Kisker et al. (Ref. 31) has very successfully brought out the features of the Fermi surface. This technique is possible to be used because the incoming photon probes the electronic states directly and hence has no severe limitations as suffered by quantum oscillatory techniques.

[31]E. Kisker, K. Schroder, M. Campagna, and W. Gudat, Phys. Rev. Lett. 52, 2285 (1984).

[32]As suggested by Mott, due to polarization of the energy bands in the magnetic phase, the d-up and d-down bands are asymmetric and hence we have two types of electron phonon scattering (in which conduction electrons are trapped at d holes), which operate in parallel. In addition, recalling that the transition metals have partially filled d bands, normal electron electron scattering between the "heavy" d electrons and the "light" sp electrons contribute to resistivity. Last but not least, unlike Heisenberg ferromagnet, in the band ferromagnet, the magnetization is a strong function of band structure. Thus the spin disorder and band structure are related. Therefore, electron magnon scattering is also correlated to the band structure.

[33]Mohammad Yousuf, P. Ch. Sahu, and K. Govinda Rajan, Pramāna 24, 825 (1985).

[34]J. F. Cannon, J. Phys. Chem. Ref. Data 3, 801 (1974).

[35]Mohammad Yousuf, P. Ch. Sahu, H. K. Jajoo, S. Rajagopalan and K. Govinda Rajan, J. Phys. F 16, 373 (1986).

[36]J. M. Leger, C. Loriers-Susse, and B. Vodar, Phys. Rev. B 6, 4250 (1972).

[37]B. Sundqvist, Solid State Commun. 37, 289 (1981).

[38]L. Kaufman, E. V. Clougherty, and R. J. Weiss, Acta Metall. 11, 323 (1963).

[39]J. M. Ziman, in Electrons and Phonons, edited by N. F. Mott, E. C. Bullard, and D. H. Wilkinson (Clarendon, Oxford, 1960), p. 377.

[40]T. L. Ruthruff, C. G. Grenier, and R. G. Goodrich, Phys. Rev. B 17, 3070 (1978).

[41]J. M. Ziman, in Electrons and Phonons, Ref. 39, p. 412.

[42]G. Grimvall, The Electron-Phonon Interaction in Metals (North-Holland, Amsterdam, 1981).

[43]J. Neve, B. Sundqvist, and O. Rapp, Phys. Rev. B 28, 629 (1983).

[44]Using the relations $v_s = (1/\hbar)(\partial E/\partial k)$ and using $\Delta k = \Gamma X = 2\pi/a = 1.785 \times 10^{10}$ m^{-1} and $\Delta E = X'_4 - \Gamma'_1 = 0.863$ Ry for spin-up sp electrons and $\Delta E = 0.862$ Ry for spin-down electrons, it is seen that $v_s^\uparrow = 0.999 \times 10^6$ m s^{-1} and $v_s^\downarrow = 0.998 \times 10^6$ m s^{-1}. Thus $v_s^\uparrow \simeq v_s^\downarrow$. Also, it is worth mentioning, at this point that these values of $v_s^\uparrow$ and $v_s^\downarrow$ are underestimates. By appropriately choosing ΔE and Δk, it is found that $v_s = 1.240 \times 10^6$ m s^{-1}.

[45]R. Joynt, J. Phys. F 14, 2363 (1984).

[46]J. Crangle and G. M. Goodman, Proc. R. Soc. London, Ser. A 321, 477 (1971).

[47]It is worth noting that the temperature dependence of ρ_{mag} above T_C can be traced to the fact that the local exchange energy and hence the local magnetic moment persists above the magnetic transition temperature and is claimed to be decreasing with temperature [D. E. Eastman, F. J. Himpsel, and J.

A. Knapp, Phys. Rev. Lett. 40, 1514 (1978)]. Consequently, it is understandable that the factor $\langle (\nabla \cdot \hat{M})^2 \rangle$ increases with temperature, leading to an increase in ρ_{mag}.

[48]F. J. Himpsel and D. E. Eastman, Phys. Rev. Lett. 41, 507 (1978).

[49]V. Korenman and R. E. Prange, Phys. Rev. Lett. 44, 1921 (1980).

[50]C. J. Maetz, U. Gerhardt, E. Dietz, A. Ziegler, and R. J. Jellito, Phys. Rev. Lett. 48, 1686 (1982).

[51]H. Hopster, R. Raue, G. Guntherodt, E. Kisker, R. Clauberg, and M. Campagna, Phys. Rev. Lett. 51, 829 (1983).

[52]J. Kirschner, M. Globl, V. Dose, and H. Scheidt, Phys. Rev. Lett. 53, 612 (1984).

[53]H. Scheidt, M. Globl, V. Dose, and D. Kirschner, Phys. Rev. Lett. 51, 1688 (1983).

[54]H. Scheidt, M. Globl, V. Dose, and D. Kirschner, J. Appl. Phys. 57, 3646 (1985).

[55]G. Grimvall, Phys. Scr. 13, 49 (1976).

[56]V. Korenman, Physica 119B, 21 (1983).

[57]V. Korenman, J. L. Murray, and R. E. Prange, Phys. Rev. B 16, 4032 (1977).

[58]D. M. Edwards, J. Magn. Magn. Mater. 15-18, 262 (1980).

[59]R. E. Prange, in Electron Correlation and Magnetism in Narrow Band Systems, edited by T. Moriya (Springer-Verlag, Berlin, 1981), p. 55.

[60]H. Hasegawa, in Electron Correlation and Magnetism in Narrow Band Systems, edited by T. Moriya (Springer-Verlag, Berlin, 1981), p. 38.

[61]J. Staunton, B. L. Gyorffy, A. J. Pindor, G. M. Stocks, and H. Winter, J. Phys. F 15, 1387 (1985).

[62]E. P. Wohlfarth, J. Magn. Magn. Mater. 45, 1 (1984); M. Cyrot, ibid. 45, 9 (1984).

[63]J. W. Lynn, Phys. Rev. B 11, 2624 (1975).

[64]H. A. Mook, J. W. Lynn, and J. M. Nicklow, Phys. Rev. Lett. 30, 556 (1973).

[65]O. Steinsvoll, C. F. Majkrazak, G. Shirane, and J. Wicksted, Phys. Rev. Lett. 51, 300 (1983).

[66]J. Wicksted, G. Shirane, and O. Steinsvoll, J. Appl. Phys. 55, 1893 (1984).

[67]H. A. Mook and J. W. Lynn, J. Appl. Phys. 57, 3006 (1985).

[68]E. Kisker, W. Gudat, E. Kuhlmann, and M. Campagna, in Recent Development in Condensed Matter Physics, edited by J. T. Devreese (Plenum, New York, 1981), p. 745 and the references therein.

[69]T. Oguchi, Prog. Theor. Phys. 13, 148 (1955).

[70]We thank Professor N. Kumar for suggesting this explanation.

[71]P. G. De Gennes and J. Friedel, J. Phys. Chem. Solids 4, 71 (1958).

[72]M. E. Fisher and J. S. Langer, Phys. Rev. Lett. 13, 665 (1968).

[73]K. P. Sinha and N. Kumar, Interactions in Magnetically Ordered Solids (Oxford University, Oxford, 1980), p. 165.

[74]V. S. Raghunathan (private communication).

[75]J. P. Bastide and C. Loriers-Susse, High Temp.—High Pressures 7, 153 (1975), and the references therein.

[76]O. Kallback, S. G. Humble, and G. Malmstrom, Phys. Rev. B 24, 5214 (1981).

[77]K. D. Jayasuriya, A. M. Stewart, S. J. Campbell, and E. S. R. Gopal, J. Phys. F 14, 1725 (1984).

[78]T. G. Kollie, Phys. Rev. B 16, 4872 (1977).